

# Chapter 2

## Quarkonium Physics

This chapter is structured as follows. Section 2.1 introduces the quarkonium spectrum, its decays, and a summary of the fields of research that use quarkonia as probes for their physics objectives. A detailed discussion of the current state-of-the-art model calculations for quarkonium production is presented in Sect. 2.2, including a historical approach to the problem, as well as comparisons of these models with data from the pre-LHC era. Finally, Sect. 2.3 will discuss recent progress regarding the analysis methodologies to be employed in measurements of quarkonium polarization.

### 2.1 Introduction

Quarkonia are bound states of a heavy quark and its respective antiquark,  $Q\bar{Q}$ , bound by the strong force. These mesons appear in two distinct “families” of states, the charmonium system, containing the mesons consisting of two charm quarks,  $c\bar{c}$ , and the bottomonium system, containing the mesons consisting of two beauty quarks,  $b\bar{b}$ .

#### Quarkonium Spectrum

The  $Q\bar{Q}$  bound system is realized in nature in many different quantum states, characterized by the quantum numbers describing the angular momentum  $L$ , the spin  $S$ , the total angular momentum  $J = S + L$ , and the principal quantum number  $N$ . Notations in the literature include both the  $J^{PC}$  convention, with parity  $P = (-1)^{(L+1)}$  and charge conjugation  $C = (-1)^{(L+S)}$ , as well as the spectroscopic notation  $N^{2S+1}L_J$ .

Figures 2.1 and 2.2 show a summary of the charmonium and bottomonium systems, respectively, showing a subset of the quarkonium states relevant for this thesis and a subset of the decays that occur within the families. Decays  $b\bar{b} \rightarrow c\bar{c}$  can be neglected [1]. These figures are restricted to CP-even states,  $J^{++}$  and  $J^{--}$ , below the open charm and open beauty thresholds. The CP-odd  $0^{-+}$  ( $\eta_c$  and  $\eta_b$ ) and  $1^{+-}$  ( $h_c$  and  $h_b$ ) states are not discussed in this thesis. The quarkonium spectra can be divided

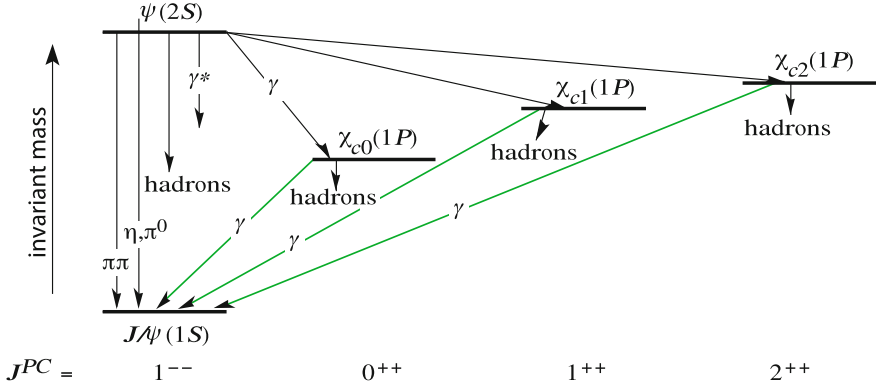


**Fig. 2.1** Charmonium spectrum and decays, adapted from Ref. [1], limited to the CP-even states below the open charm threshold

in two main categories, characterized by two different experimental signatures, the “S-wave” ( $L = 0$ ) and “P-wave” ( $L = 1$ ) states.<sup>1</sup> The S-wave states are the  $J^{PC} = 1^{--}$  vector mesons  $J/\psi$  and  $\Upsilon(1S)$ , and their radial excitations  $\psi(2S)$ <sup>2</sup> and the  $\Upsilon(2S)$  and  $\Upsilon(3S)$  mesons, respectively. The two charmonium S-wave states are referred to as  $\psi(nS)$  (with  $n = 1, 2$ ) states, while the three S-wave bottomonium states are denoted as  $\Upsilon(nS)$  (with  $n = 1, 2, 3$ ) states. The P-wave states are the  $J^{PC} = J^{++}$  pseudo vector mesons  $\chi_{cJ}$  and  $\chi_{bJ}(1P)$  that appear in triplets corresponding to  $J = 1, 2, 3$  and their radial excitations, in the case of the bottomonium system, the  $\chi_{bJ}(2P)$  and  $\chi_{bJ}(3P)$ . Experimentally, the most important decay modes are the “dimuon” decays of the S-wave states,  $\psi(nS) \rightarrow \mu\mu$  and  $\Upsilon(nS) \rightarrow \mu\mu$ , and the radiative decays of the P-wave states,  $\chi_{cJ} \rightarrow J/\psi + \gamma$  and  $\chi_{bJ}(nP) \rightarrow \Upsilon(mS) + \gamma$ .

Detailed listings of the particle masses, full widths, decay modes and the corresponding branching fractions can be found in Ref. [1]. For the charmonium system, the masses cover the range from 3.0969 GeV of the  $J/\psi$  up to 3.6861 GeV for the  $\psi(2S)$ ; in the bottomonium system the masses cover the range from 9.4603 GeV<sup>3</sup> for the  $\chi_b(3P)$ . The full widths of the quarkonium states are small compared to experimental resolution, except for the  $\chi_{cJ}$  states, with widths of 10.3, 0.86 and 1.97 MeV, respectively for the  $\chi_{c0}$ ,  $\chi_{c1}$  and  $\chi_{c2}$  states, while the widths of the  $\chi_{bJ}(nP)$  states are yet to be measured. The decay times of the S-wave states are in the range of  $2\text{--}40 \times 10^{-21}$  s, while the decay times of the P-wave states (in the charmonium cases, where they are measured) are in the range  $6\text{--}70 \times 10^{-23}$  s. With these decay times, the quarkonium states only travel average distances of the order of femto- up to pico-meters, before they decay. All the quarkonium decays are therefore classified as “prompt” (quasi-instantaneous, PR) decays.

<sup>1</sup>In this thesis, the terms “S-wave” and “P-wave” states only refer to CP-even states.

<sup>2</sup>The  $\psi(2S)$  state is also referred to as  $\psi'$  in the literature.

<sup>3</sup>This PDG [1] mass value will be updated with recent LHCb results [2, 3].

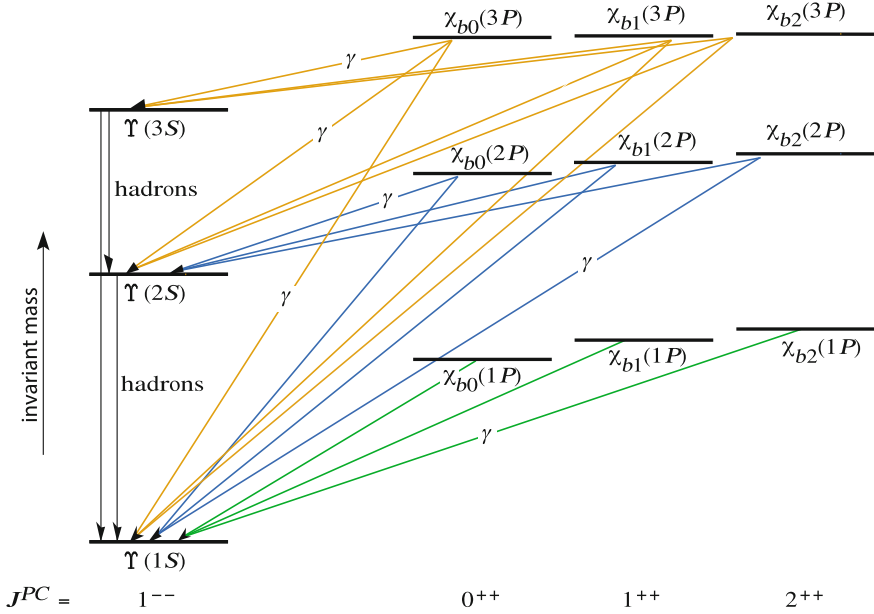


**Fig. 2.2** Bottomonium spectrum and decays, adapted from Ref. [1], limited to the CP-even states below the open beauty threshold. Decays of the type  $\Upsilon(nS) \rightarrow \chi_{bJ}(mP) + \gamma$  are not shown

At this point it should be mentioned that natural units are used in this thesis, with  $\hbar = c = 1$ , therefore giving energy, mass and momentum in units of eV.

The experimental samples of S-wave and P-wave events are a mixture of directly produced quarkonia and products of the decays from heavier states, so-called “feed-down decays”. While it is possible to separate, experimentally, samples of P-wave states, by requesting a  $\gamma$  in the final state, it is not (currently) possible, due to the short decay times of quarkonia, to separate the directly produced S-wave states from the feed-down decays. The experimental measurements of S-wave states are therefore limited to the measurement of the properties of the prompt components, not removing the feed-down contributions. The same is true for the P-wave states, which are also affected by feed-down decays from radiative transitions from the S-wave states. However, by measuring the properties of the feed-down states, connected with knowledge about the “feed-down fractions”, defining the mixture of the production channels of the prompt samples, the properties of the directly produced quarkonium states are accessible a posteriori, in the interpretation of the measurements.

The highest-mass charmonium and bottomonium states, the  $\psi(2S)$  and  $\chi_b(3P)$  states, are considered to be free of feed-down decays, hence the measurement of the respective prompt samples allows access to the directly produced quarkonium states. The corresponding measurements are therefore especially important, given that the comparison with model calculations is simplified thanks to the experimentally very clear information. The  $\Upsilon(3S)$  state has been regarded as feed-down free for several

decades, until recently, due to the discovery of the  $\chi_b(3P)$  state by the ATLAS Collaboration in the  $\chi_b(3P) \rightarrow \Upsilon(1S) + \gamma$  and  $\chi_b(3P) \rightarrow \Upsilon(2S) + \gamma$  decays [4], the confirmation by the D0 Collaboration in the  $\chi_b(3P) \rightarrow \Upsilon(1S) + \gamma$  decay [5], and the measurement of the feed-down fractions of the  $\chi_b(3P) \rightarrow \Upsilon(nS) + \gamma$  by the LHCb Collaboration [2], including the first observation of the  $\chi_b(3P) \rightarrow \Upsilon(3S) + \gamma$  decay. The corresponding estimate of the feed-down fraction is affected by large uncertainties, but the data reveal that more than 1/3 of  $\Upsilon(3S)$  mesons produced at the LHC originate through the radiative  $\chi_b(3P) \rightarrow \Upsilon(3S) + \gamma$  transition. While it has not been established experimentally that the  $\chi_b(3P)$  state is in fact the third radial excitation of the  $\chi_{bj}(1P)$  triplet, with a triplet substructure of  $J = 1, 2, 3$  states, with the  $J^{PC}$  states  $0^{++}$ ,  $1^{++}$  and  $2^{++}$ ,  $\chi_{bj}(3P)$ , this is regarded as very likely within the scientific community. This assumption is reflected in Fig. 2.2, therefore to be interpreted and used with care.

### Quarkonia as Probes

Quarkonium mesons are studied by various scientific communities, in several collision systems, motivated by very different considerations. Here, the most important aspects are summarized briefly, to emphasize the wealth of possibilities in quarkonium physics. More details on all mentioned topics can be found in Ref. [6].

Quarkonium spectroscopy and decays constitute active fields of research. The spectrum of “conventional” quarkonia, as discussed above, is rather well understood. With the exception of the  $\chi_b(3P)$  discovery and subsequent studies regarding the nature (triplet-substructure) of this state, a more accurate measurement of its mass, and an assessment of the branching fractions of its decays, the chapter of conventional quarkonium spectroscopy can be regarded as closed. However, there is a wealth of studies ongoing, both at b-factory experiments and hadron collider experiments, in the field of so-called “exotic quarkonium” physics. In the last decade, several such exotic quarkonium states have been discovered, and their quantum states determined, often through decays involving the  $\psi(nS)$  and  $\Upsilon(nS)$  quarkonium states. The first and most famous of these states is the neutral  $X(3872)$ , first discovered by the Belle Collaboration [7] and confirmed by several other collaborations. The LHCb Collaboration has measured the quantum numbers of this state to be  $J^{PC} = 1^{++}$ , in the decay  $X(3872) \rightarrow J/\psi \pi \pi$  [8]. The properties of the  $X(3872)$ , as measured by the individual experiments, do not fit the expectations of a simple charmonium state. The nature of this state is still unclear. The exciting possible explanations include a loosely-bound molecule of two mesons, as well as a tightly-bound diquark-diantiquark bound system, which would require the existence of two neutral and one charged partner state, which have not been established yet, experimentally [6]. A further very interesting state is the charged  $Z(4430)^\pm$ , discovered by the Belle Collaboration [9] and confirmed by the LHCb Collaboration [10]. The confirmation of this state has attracted attention of a wide range of the physics community, as the minimal quark content of such a charged state is  $c\bar{c}d\bar{u}$  [10]. This can be viewed as the first unambiguous evidence for hadrons with more than the traditional  $q\bar{q}$  or  $qqq/\bar{q}\bar{q}\bar{q}$  content, which was already proposed by Gell-Mann, in the original paper introducing quarks as the fundamental constituents of all hadrons [11].

Quarkonia also play a major role in experiments studying hot and dense QCD matter with heavy-ion (HI) collisions. In these collisions, at very high energy densities, a phase transition to a quark gluon plasma (QGP) is expected to occur. Quarkonia are produced very early in the collisions, prior to formation of the QGP. Their evolution through the medium produced in the HI collisions can provide information about the QGP. Due to a Debye screening of the QCD potential binding the  $Q\bar{Q}$  pairs, quarkonia are expected to be “melted” in the hot medium [12]. Given that the individual quarkonia have very different binding energies, increasing with the difference of the quarkonium mass with respect to the open charm/beauty thresholds, the individual quarkonium states melt at different energy densities of the collisions. The higher-mass states get suppressed at lower energy densities than the lower-mass states, which are more tightly-bound. Therefore, one expects a sequential suppression of the quarkonium states as a function of the energy density [13], a smoking gun signal for QGP, affecting also the lower-mass states due to the suppression of the feed-down contributions. However, at the LHC other effects complicate the interpretation of the results, such as recombination [14], where due to the high abundance of charm quarks in the collisions,  $c$  and  $\bar{c}$  quarks produced in different nucleon-nucleon collisions bind together forming a charmonium state.

There are several other fields that use quarkonia as probes, which will not be discussed in more detail here. These topics include for example the measurement of CP violating phases in B-hadron decays, which often involve  $\psi(nS)$  mesons in their final state signatures. Other interesting decays, which are however by far not yet accessible with the data samples collected by the LHC experiments, are the Higgs decays  $H \rightarrow J/\psi + \gamma$  and  $H \rightarrow \Upsilon(1S) + \gamma$ , from which the  $Hc\bar{c}$  and  $Hb\bar{b}$  couplings can be measured [15].

Finally, motivating the research presented in this thesis, a detailed understanding of the fundamental mechanisms that lead to the production of quarkonia helps to understand hadron formation in general, which is not yet well understood in the SM, and is therefore an active field of research in both experiment and theory. The corresponding strategies for the model calculations of quarkonium production observables, including quarkonium cross sections and polarizations, are discussed in detail below.

## 2.2 Quarkonium Production

Due to their simple and symmetric composition, as well as to the heavy quark masses  $m_Q$ , heavy quarkonium states are ideal laboratories to test the interplay between perturbative and non-perturbative QCD. A detailed understanding of quarkonium production helps to understand hadron formation, how the strong interaction binds quarks into hadrons.

One basic concept guides all considerations regarding the understanding of quarkonium production. The production of any quarkonium state is assumed to be factorizable in two parts. The first part is the production of an intermediate  $Q\bar{Q}$  pair at

short distance, which is calculable within perturbative QCD and is fairly well understood. The second part is the hadronization, the intermediate  $Q\bar{Q}$  pair forming a QCD bound quarkonium state. This stage of the production is part of the non-perturbative realm of QCD, which causes problems in the modeling and the understanding of quarkonium production.

Quarkonia can be treated as approximately non-relativistic systems, given the heavy quark masses and the resulting relative quark velocity  $v$  in the bound state, with  $v^2 \approx 0.3$  for the charmonium and  $v^2 \approx 0.1$  for the bottomonium states [6]. Due to the relatively small heavy-quark velocities, the two factorized steps occur at distinct timescales. The time needed for the production of the  $Q\bar{Q}$  pair is proportional to  $1/m_Q$ , while the non-perturbative formation of the bound state occurs at a time scale of the order of  $1/(m_Q v^2)$  [16]. If these two timescales are well separated, which is the case if  $1/(m_Q v^2) \gg 1/m_Q$ , the intuitive expectation is that the short-distance and long-distance effects can indeed be separated. While this condition is well fulfilled for bottomonium states, and reasonably well for charmonium states, this is not the case, for example, for light hadrons, where the two production steps cannot be factorized in two distinct processes that occur at different time scales. For these reasons, quarkonia provide a unique opportunity to study hadron formation, and to learn about the interaction dynamics involving the long-distance strong force.

Full QCD calculations of quarkonium production observables are limited to the perturbative part of quarkonium production, up to certain powers in  $\alpha_s$ . The non-perturbative formation of the bound state is not calculable with perturbative approaches. This part would, in principle, be accessible by calculations within the framework of lattice QCD, but such an effort has not yet been performed. Therefore, current calculations for quarkonium production have to rely on certain assumptions and approximations. There are several different models, attempting to calculate quarkonium production observables, with various levels of success of reconciling data and model calculations. There is wide consensus in the scientific community that the NRQCD factorization approach currently provides the most reliable calculations, with the best chances of successfully describing simultaneously all available quarkonium production measurements. Therefore, this model is introduced in detail below, while other models, that would nevertheless deserve the attention of the reader, are not discussed here, but are summarized in Ref. [6]. The Color-Singlet Model (CSM) is included in the NRQCD factorization approach as a special case. The alternative approaches, not discussed here, include the Color-Evaporation Model (CEM), introduced in [17], and the  $k_T$  factorization approach [6].

### 2.2.1 Non-relativistic QCD Factorization

NRQCD is an effective field theory that was introduced in Ref. [16]. NRQCD, in general, can be regarded as a direct consequence of full QCD, in the limit of  $m_Q \rightarrow \infty$ . However, the approach relies heavily on the validity of the factorization of the production of the initial  $Q\bar{Q}$  pair, and the formation of the bound state. In the framework

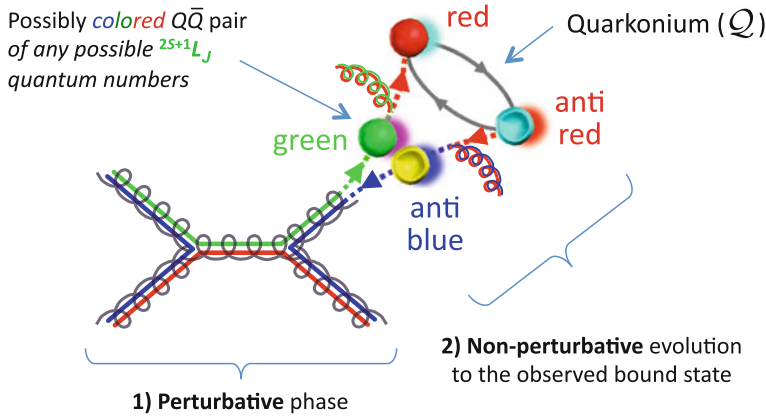


**Fig. 2.3** Sketch illustrating the two distinct steps of quarkonium production: the perturbative production of an initial possibly colored  $Q\bar{Q}$  pair, followed by the formation of a color-neutral quarkonium state  $Q$  via the non-perturbative emission of soft gluons [18]

of NRQCD, the cross section  $\sigma(Q)$  of the quarkonium  $Q$  can be calculated by the simple factorization formula [16]

$$\sigma(Q) = \sum_n \mathcal{S}[Q\bar{Q}(n)] \cdot \mathcal{O}^Q(n). \quad (2.1)$$

The calculation is factorized in the short-distance coefficients (SDC)  $\mathcal{S}[Q\bar{Q}(n)]$ , describing the perturbative production of the initial  $Q\bar{Q}$  pair in quantum state  $n = ^{2S+1}L_J^{[C]}$ , with  $C$  the color multiplicity, and the long-distance matrix elements  $\mathcal{O}^Q(n)$ , describing the non-perturbative evolution into the bound quarkonium  $Q$  in state  $n'$ ,  $Q^{n'}$ . The individual terms of this sum, characterized by the various intermediate states  $n$  are denoted as the “partial cross sections”  $\sigma(n) = \mathcal{S}[Q\bar{Q}(n)] \cdot \mathcal{O}^Q(n)$ . The sum of the partial cross sections runs over all possible intermediate  $Q\bar{Q}$  states  $n$ , including color-singlet (CS,  $C = 1$ ) and color-octet (CO,  $C = 8$ ) configurations. This formalism allows the existence of intermediate CO states in nature, with transitions into the physical color-neutral quarkonium bound state via the non-perturbative emission of soft gluons, as is illustrated in Fig. 2.3.

### Short-Distance Coefficients

The SDCs  $\mathcal{S}[Q\bar{Q}(n)]$  can be calculated with perturbative QCD approaches, as expansion in powers of  $\alpha_s$ , and correspond to the sum of the partonic cross sections to produce a  $Q\bar{Q}$  pair in state  $n$ , convoluted with the parton distribution functions. The SDCs are functions accounting for the kinematic dependence of the cross section and decay distributions and are process dependent, different for any collision system and CM energy. As this thesis discusses measurements at the LHC, considerations are restricted to SDCs calculated for  $pp$  collisions.

The polarization parameters  $\vec{\lambda} = (\lambda_\vartheta, \lambda_\varphi, \lambda_{\vartheta\varphi})$ , with respect to a certain quantization axis  $z$  (see Sect. 2.3), can be calculated by defining the SDCs corresponding to the individual projections of the  $Q\bar{Q}$  spin  $S$  on the quantization axis  $z$ ,  $S_{ij}[Q\bar{Q}(n)] (= S_{ij})$ , with the notation  $i, j = 0, \pm 1$  [19],

$$\lambda_\vartheta = \frac{S_{11} - S_{00}}{S_{11} + S_{00}}, \quad \lambda_\varphi = \frac{S_{1,-1}}{S_{11} + S_{00}}, \quad \lambda_{\vartheta\varphi} = \frac{\sqrt{2}\text{Re}S_{10}}{S_{11} + S_{00}}, \quad (2.2)$$

with  $S_{11}$  being the “transverse SDC” and  $S_{00}$  the “longitudinal SDC”. The total SDC is given by the relation  $S[Q\bar{Q}(n)] = S_{00}[Q\bar{Q}(n)] + 2 \cdot S_{11}[Q\bar{Q}(n)]$ .

### Long-Distance Matrix Elements

The LDMEs  $\mathcal{O}^Q(n)$  can be intuitively understood as being proportional to the probability of a given intermediate  $Q\bar{Q}$  in state  $n$  to form a quarkonium state  $Q$ . They are constants, independent of the  $Q\bar{Q}$  kinematics, and are assumed to be universal, identical for any collision system, only depending on the initial  $Q\bar{Q}$  state  $n$  and the final state  $Q$ . The LDMEs are not calculable with currently available techniques (with the exception of the CS LDMEs, see below), and have to be estimated by fits to experimental data, discussed in more detail in Sects. 2.2.2 and 5.2.

In principle, one would have to sum over all possible intermediate states  $n$  in order to calculate the full, “color-inclusive” cross sections and polarizations of the individual quarkonium states  $Q$ . However, the individual LDMEs can be organized in certain hierarchies, “power-counting schemes” or “velocity scaling rules”, which estimate the relative size of the individual LDMEs in powers of the heavy-quark velocity  $v$ . There are various slightly differing suggestions for these hierarchies in the literature. A fairly common definition of the importance of the individual LDMEs follows the relation [20]

$$\mathcal{O}^Q(n) \propto v^{2L+2E_1+4M_1}, \quad (2.3)$$

with  $L$  the angular momentum of the  $Q\bar{Q}$  state,  $E_1$  the minimum number of chromoelectric ( $\Delta L = \pm 1, \Delta S = 0$ ) transitions necessary to reach the quarkonium state  $Q$  from the  $Q\bar{Q}$  state  $n$ , and  $M_1$  the minimum number of chromomagnetic ( $\Delta L = 0, \Delta S = \pm 1$ ) transitions. Table 2.1 summarizes the most important states  $n$  and the corresponding expected suppression, in powers of  $v$ , following these velocity scaling rules, separately for S-wave  $1^{--}$  and P-wave  $J^{++}$  states. This table includes CO intermediate states, as well as CS transitions with  $S, L$  and  $J$  configurations different from those of the final state  $Q$ , which are clearly suppressed and not considered in the CSM.

Due to the small velocities  $v$  in the heavy quarkonium states, the partial cross sections of the states characterized by large powers of  $v$  are expected to be negligible with respect to the leading ones. It has to be emphasized that even though the LDMEs of velocity scaling suppressed states  $n$  are expected to be small, this could in principle be compensated by large values of the corresponding SDCs. However, the standard approach is to only consider in the sum over intermediate  $Q\bar{Q}$  states



**Table 2.1** Expected scaling of the LDMEs  $\mathcal{O}^{\mathcal{Q}}(n)$ , in powers of  $v$ , for  $1^{--}$  and  $J^{++}$  states [20]

CS states $n$	$^1S_0^{[1]}$	$^3S_1^{[1]}$	$^1P_1^{[1]}$	$^3P_J^{[1]}$	$^3D_J^{[1]}$	$^1D_2^{[1]}$
$\mathcal{Q} = 1^{--}$	$v^8$	<b>1</b>	$v^8$	$v^8$	$v^8$	$v^{12}$
$\mathcal{Q} = J^{++}$	$v^6$	$v^6$	$v^{10}$	<b><math>v^2</math></b>	$v^{10}$	$v^{10}$
CO states $n$	$^1S_0^{[8]}$	$^3S_1^{[8]}$	$^1P_1^{[8]}$	$^3P_J^{[8]}$	$^3D_J^{[8]}$	$^1D_2^{[8]}$
$\mathcal{Q} = 1^{--}$	<b><math>v^4</math></b>	<b><math>v^4</math></b>	$v^8$	<b><math>v^4</math></b>	$v^8$	$v^{12}$
$\mathcal{Q} = J^{++}$	$v^6$	<b><math>v^2</math></b>	$v^6$	$v^6$	$v^6$	$v^{10}$

$n$  (Eq. 2.1) the states whose expected velocity scaling goes up to and including  $v^4$ . This approach is well justified for bottomonium states, due to the heavy mass of the beauty quark. However, it remains to be seen if these scaling rules are applicable also for charmonium states, with a considerably larger  $v$ . These considerations lead to the commonly considered intermediate states  $^3S_1^{[1]}$ ,  $^1S_0^{[8]}$ ,  $^3S_1^{[8]}$  and  $^3P_J^{[8]}$  for S-wave  $1^{--}$  quarkonia, and the intermediate states  $^3P_J^{[1]}$  and  $^3S_1^{[8]}$  for P-wave  $J^{++}$  quarkonia. The actually considered terms differ in the individual NRQCD analyses, as detailed in Sect. 5.2.

### Color-Singlet Model as Special Case of the NRQCD Factorization Approach

The CSM can be obtained as a special case of the NRQCD factorization approach, if in Eq. 2.1 only the CS term is considered, which is characterized by identical states  $n$  and  $\mathcal{Q}$ . In this case, for S-wave  $1^{--}$  quarkonia only the  $^3S_1^{[1]}$  intermediate state is considered, while for P-wave  $J^{++}$  quarkonia only the  $^3P_J^{[1]}$  state is considered. Considering the CSM alone leads to infrared divergencies in the case of the calculation of the cross sections of  $J^{++}$  quarkonia, which can only be compensated by the addition of CO terms [16].

Due to the simplicity of the transition of the CS  $Q\bar{Q}$  state into the quarkonium state  $\mathcal{Q}$  ( $\Delta L = 0$ ,  $\Delta S = 0$ , no non-perturbative emission of soft gluons), the CS LDMEs can be calculated with high precision in several ways, including potential model approaches [6], and determined experimentally, through the measurement of the decay widths of the quarkonium states, given the known relations between the production and decay matrix elements [21].

### Status of NRQCD Calculations

Full NRQCD calculations exist at LO in  $\alpha_s$  and NLO, for various quarkonium states, CS and CO channels, collision systems, kinematic regions and center-of-mass energies. The ones relevant for this work can be found in Refs. [19, 22–27]. Figure 2.4 shows dominant LO diagrams for the hadroproduction of  $1^{--}$  quarkonia for the  $^3S_1^{[1]}$  CS channel (left), the dominating gluon fragmentation diagram for the  $^3S_1^{[8]}$  CO channel (middle), and a LO diagram for the  $^1S_0^{[8]}$  and  $^3P_J^{[8]}$  CO channels (right).

These perturbative QCD calculations are provided as a function of the quarkonium kinematics in the laboratory frame. In collider experiments it is common to use the

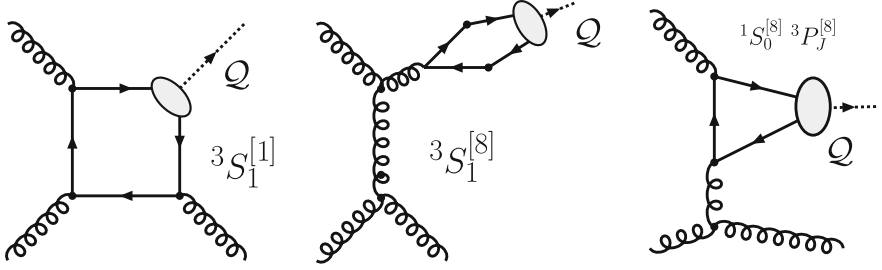


**Fig. 2.4** LO diagrams for the hadroproduction of  $1^{--}$  quarkonia  $Q$  for the  $^3S_1^{[1]}$  CS channel (left), for the  $^3S_1^{[8]}$  CO channel (middle), and for the  $^1S_0^{[8]}$  and  $^3P_J^{[8]}$  CO channels (right) [6]

transverse momentum  $p_T$  and the rapidity  $y$ , defined as

$$y = \frac{1}{2} \ln \left( \frac{E + p_L}{E - p_L} \right), \quad (2.4)$$

with  $E$  the particle energy and  $p_L$  the longitudinal momentum, along the beam-axis. Regions in phase space close to  $|y| = 0$  are referred to as “mid-rapidity” regions, contrary to “forward-rapidity” regions, characterized by larger values of  $|y|$ .

Figure 2.5 shows an example of such NRQCD calculations, as taken from Ref. [19], for  $J/\psi$  production in  $pp$  collisions at  $\sqrt{s} = 7$  TeV at mid-rapidity, as a function of  $p_T$ . The top left panel shows the SDCs at NLO. The top right panel shows the ratio of the SDCs at NLO with respect to the LO calculations, indicating the relative change between the LO and NLO calculations. This ratio is denoted as the SDC “k-factor”. The bottom panel shows the polarization parameter  $\lambda_\theta$  in the Helicity (HX) frame at NLO. The polarization parameters and reference frames are defined in Sect. 2.3. These calculations are made for  $|y| < 0.9$ , but the calculations [19] have shown that the SDCs and polarizations of the individual color channels change only marginally with rapidity.

At NLO, the individual color channels have very different polarizations, ranging from almost fully longitudinal ( $^3S_1^{[1]}$ ), unpolarized ( $^1S_0^{[8]}$ ), almost fully transverse  $^3S_1^{[8]}$  to “hyper-transverse” ( $^3P_J^{[8]}$ ), with a divergent behavior and a change of sign at  $p_T \approx 9$  GeV. Above a certain  $p_T$  of approximately 15 GeV the polarizations at NLO can be regarded as constant. The shapes of the  $p_T$ -differential SDCs at NLO are rather similar for the individual color channels, albeit characterized by different levels of steepness of the curves as a function of  $p_T$ , the  $^3S_1^{[1]}$  being the steepest, and the  $^3S_1^{[8]}$  and  $^3P_J^{[8]}$  being the flattest, towards high  $p_T$ . The NLO SDC of the  $^3P_J^{[8]}$  is positive at low  $p_T$  and changes sign at around 7 GeV (not visible in the top left panel of Fig. 2.5 due to the shown range in  $p_T$ ).

Comparing the behavior at LO and NLO one can observe that the  $^3S_1^{[8]}$  and  $^1S_0^{[8]}$  are very stable in the perturbative expansion, with small SDC k-factors and no changes in polarization [19]. On the contrary, the  $^3S_1^{[1]}$  and  $^3P_J^{[8]}$  channels show very large

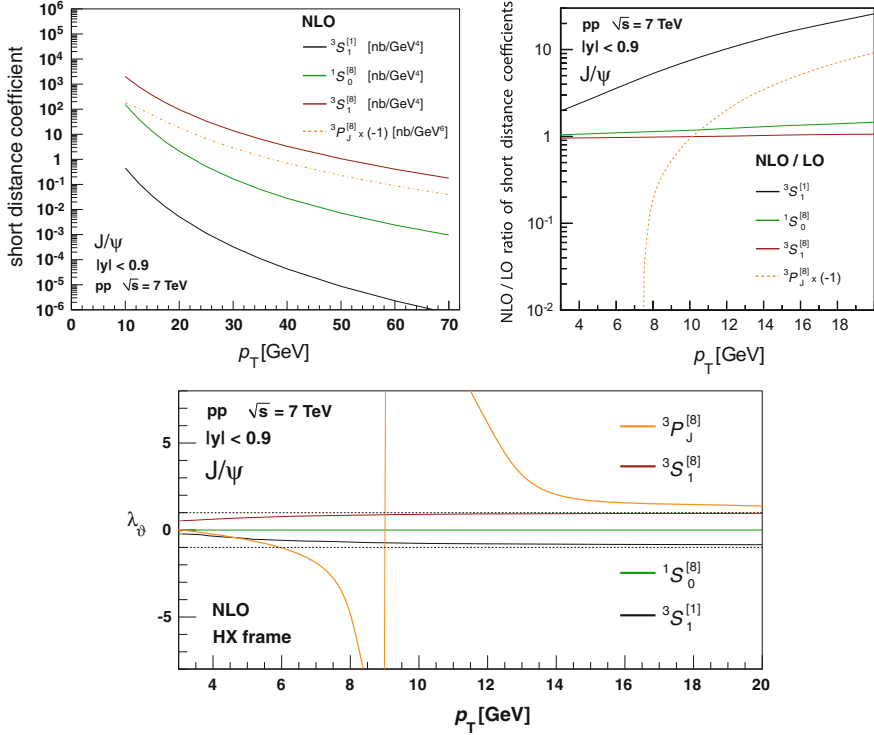


**Fig. 2.5** NRQCD calculations [19] for  $J/\psi$  production in  $pp$  collisions at  $\sqrt{s} = 7$  TeV at mid-rapidity, as a function of  $p_T$ , showing the SDCs at NLO (*top left*), the ratio of the SDCs at NLO with respect to the LO calculations (*top right*) and the polarization parameter  $\lambda_\theta^{HX}$  at NLO (*bottom*)

changes, indicating that the perturbative expansion in  $\alpha_s$  is not yet convergent at NLO. Furthermore, the polarization parameter  $\lambda_\theta$  changes from almost fully transverse at LO to almost fully longitudinal at NLO for the  $^3S_1^{[1]}$  channel. For the  $^3P_J^{[8]}$  channel,  $\lambda_\theta$  changes from the unpolarized scenario at LO to a hyper-transverse polarization at NLO [19]. Given the large SDC k-factors of the  $^3S_1^{[1]}$  and  $^3P_J^{[8]}$  channels, it would be desirable to have access to calculations of higher-order QCD corrections, at next-to-next-to-leading order (NNLO), or even beyond. However, full NNLO calculations are beyond the scope of the techniques currently used. For the CS  $^3S_1^{[1]}$  channel there has been a large effort to calculate partial NNLO corrections, denoted as NNLO\* [28, 29]. These calculations take into account processes where the  $1^{--}$  quarkonium is produced in association with three light partons, which are assumed, by the authors, to be the dominantly contributing processes at NNLO. The success of describing hadron collider quarkonium production data with this model, among others, is discussed below.

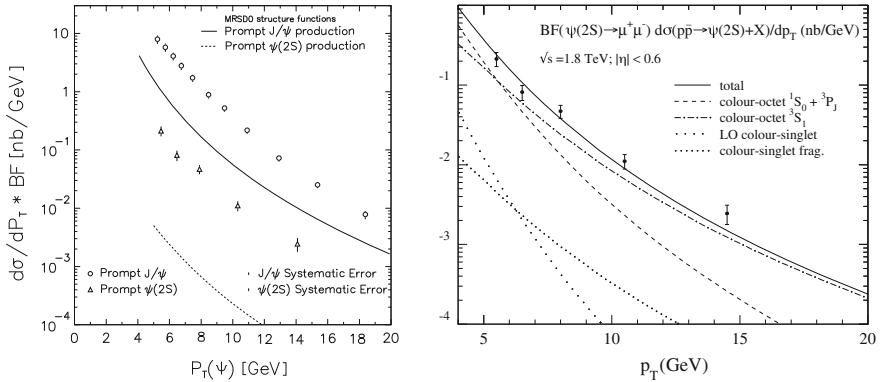


**Fig. 2.6** Production cross sections of prompt  $J/\psi$  and  $\psi(2S)$  mesons as measured by the CDF Collaboration, as a function of  $p_T$ , compared to curves based on LO CSM calculations [37] (left). Production cross sections of prompt  $\psi(2S)$  mesons as measured at CDF [37], compared to LO NRQCD calculations [38] (right)

### 2.2.2 Quarkonium Production in the Pre-LHC Era

The history of quarkonium physics has been accompanied by several long-standing problems, including several experimental inconsistencies. At this point, it is useful to illustrate in a few paragraphs the chronological developments in the field of quarkonium production, in order to understand its status in the pre-LHC era, and to appreciate the level of progress made thanks to the excellent performance of the LHC experiments and the simultaneous progress in the context of NRQCD.

The discovery of the  $J/\psi$  meson, simultaneously in  $p + Be$  collisions at BNL [30] and in  $e^+e^-$  collisions at SLAC [31], was the first experimental sign of the charm quark, and opened up a new field in particle physics research, which is still actively followed in the LHC era.

Few years after the discovery, the intuitive and simple CSM was developed [32–34], with the ability to calculate quarkonium cross sections, differential in transverse momentum, without the need for free parameters that have to be fit to the data, as is the case in NRQCD. This CSM was first challenged by measurements of  $J/\psi$  and  $\psi(2S)$  cross sections by fixed-target experiments at Fermilab [35, 36], which exceeded the CSM predictions (at LO, at that time) by large factors. This was not regarded as a serious problem, especially for the  $J/\psi$ , which is affected by the – at that time – completely unknown feed-down fractions from heavier charmonium states. These measurements were made at relatively low values of  $p_T$ , where non-perturbative effects were also expected to justify differences between the data and the CSM curves.

The situation changed after the first measurements of quarkonium production cross sections at the Tevatron experiments, which could access much higher values of  $p_T$  than previously explored, entering regions where  $p_T \gg M_\psi$ , with  $M_\psi$  the mass

of the quarkonium state  $Q$ . The measured production cross sections of the prompt  $\psi(nS)$ ,  $\Upsilon(nS)$  [37, 39] and  $\chi_c$  [40] quarkonia were once again large factors above the LO CSM calculations, as can be seen, in the case of the  $\psi(nS)$ , in the left panel of Fig. 2.6. At this point, the scientific community was alarmed, especially due to the  $\psi(2S)$  discrepancy, which could not be attributed to any feed-down decays, the CSM underestimating the observed yields by a factor of 40–50, a problem also known as the “ $\psi(2S)$  anomaly”.

Roughly at that time, the NRQCD factorization approach was born [16]. The SDCs were first calculated at LO, and tested on Tevatron quarkonium cross section data. The  $\psi(2S)$  anomaly could be successfully solved by adding CO contributions on top of the CS calculations, with free fit parameters representing the LDMEs of the individual CO contributions. The resulting fit could nicely describe the CDF  $\psi(2S)$  data, as can be appreciated in the right panel of Fig. 2.6.

Despite the success of the LO NRQCD calculations, the trust in these new calculations was limited, given the enormous freedom of the model, with the overall normalization of the production cross section given by free parameters of the fit, and the shape of the distribution given by the relative importance of the individual color channels, characterized by  $p_T$ -distributions of different slopes. The obvious next step was to predict other measurable observables within the framework of NRQCD, and to measure them experimentally. The LDMEs fitted from the cross section measurements can be used to predict the polarization of the inclusive sample, built from color channels with different polarizations, with relative weights proportional to the LDMEs. With this approach, several groups conducting LO NRQCD calculations predicted almost fully transverse polarization in the HX frame, especially at high  $p_T$ , for Tevatron  $J/\psi$  and  $\psi(2S)$  production (see Ref. [41] and references therein). However, the CDF Collaboration measured no large polarizations [42, 43]. The CDF results for prompt  $J/\psi$  and  $\psi(2S)$  polarizations [43] are compared to the LO NRQCD calculations from Ref. [41] in Fig. 2.7. The  $J/\psi$  prediction for  $\lambda_\theta$  includes feed-down effects from the  $\psi(2S)$  and  $\chi_{cJ}$  states, and can therefore be directly compared to the prompt measurement of the CDF Collaboration. The measurements of both the  $J/\psi$  and  $\psi(2S)$  polarizations are in clear disagreement with the LO NRQCD calculations, challenging their validity.

### Puzzles and Solutions

The disagreement of the LO NRQCD calculations and the Tevatron quarkonium polarization measurements was often referred to as the “quarkonium polarization puzzle”, which received a lot of attention by the scientific community, and several approaches were tested to solve the problem. One attempt was to extend the LO calculations of NRQCD to NLO, a task performed by several groups [19, 22–27].

The analysis described in Ref. [44] was among the first to use NLO NRQCD calculations to attempt a fit to extract the LDMEs for  $J/\psi$  production. Production cross section measurements from both hadroproduction, including early LHC measurements, and photoproduction at HERA were studied to extract the LDMEs, which were then used to predict the  $J/\psi$  polarization. More details about this analysis – and several other similar NRQCD analyses – can be found in Sect. 5.2. The analysis was

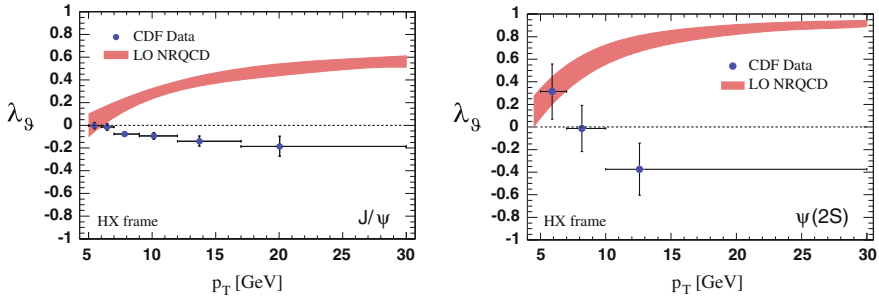


**Fig. 2.7** Prompt  $J/\psi$  (left) and  $\psi(2S)$  (right) polarization parameter  $\lambda_\theta$  measured in the HX frame by the CDF Collaboration [43], compared to LO NRQCD calculations [41]

a success in the sense that the production cross sections of different collision systems could be reproduced simultaneously, hinting at the validity of the universality claim of the NRQCD factorization approach. However, the predicted  $J/\psi$  polarization was very similar to the LO predictions, almost fully transverse in the HX frame, especially at high  $p_T$ . Therefore, the CDF polarization measurements could not be explained by these NLO NRQCD calculations.

The large differences between the CS LO and NLO calculations opened the possibility that the full CS quarkonium cross sections could be large enough to describe the data (or ensure that only a rather small CO component is needed). The NNLO\* calculations described above were compared to the available data, for both cross section and polarization measurements [28, 45]. The  $J/\psi$  and  $\Upsilon(nS)$  cross sections for CS NNLO\* calculations do not describe the data, which are systematically above the calculations. The CS NNLO\* polarizations are similar to the CS NLO calculations, but slightly more longitudinal. Therefore, these calculations cannot describe the mostly unpolarized CDF  $J/\psi$  data. However, this comparison is not entirely fair given that the CS NNLO\* calculations do not include feed-down decays. Nevertheless, the CS NNLO\* calculations supported the idea that CO contributions are indeed necessary to explain quarkonium production data.

One further unfortunate but important component of the quarkonium polarization story of the pre-LHC era are a series of experimental inconsistencies. The Tevatron experiments have published results for quarkonium polarization which are mutually inconsistent, as illustrated in Fig. 2.8. The left panel shows CDF measurements of the prompt  $J/\psi$  polarization in the HX frame from data taken in different run periods [42, 43]. The slight change in CM energy from  $\sqrt{s} = 1.8$  TeV to  $\sqrt{s} = 1.96$  TeV, as well as the slight difference in the rapidity regions of the measurements cannot explain the large differences among the results. The right panel shows measurements of the  $\Upsilon(1S)$  polarization in the HX frame as measured at  $\sqrt{s} = 1.96$  TeV by the CDF Collaboration [46] and the D0 Collaboration [47]. Also in this case one can see a large discrepancy, which again cannot be explained by the different rapidity regions of the measurements.

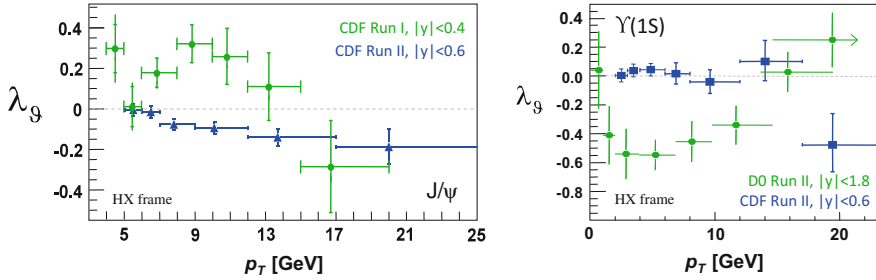


**Fig. 2.8** Measurements of the polarization parameter  $\lambda_\theta$  in the HX frame, for the prompt  $J/\psi$  by the CDF Collaboration [42, 43] (left) and for the  $\Upsilon(1S)$  by the CDF Collaboration [46] and the D0 Collaboration [47] (right)

Given that the data could not be fully trusted, the disagreement with the LO NRQCD calculations was not regarded as a major problem in the pre-LHC era. These unfortunate inconsistencies are the main reason why quarkonium polarization measurements were not considered in the NRQCD fits of the LDMEs, but rather used as a check to compare the NRQCD predictions for the polarization observables, which are obtained a-posteriori. This is especially inauspicious as the polarization observables, given the clear differences between the individual color channels, give more intuitive information about the relative importance of the channels than the differential cross sections, which are relatively similar for all underlying processes.

At this point, it can only be speculated why the Tevatron era was affected by such inconsistencies. Due to progress in the understanding of quarkonium polarization (see Sect. 2.3), it is now clear that 1-dimensional angular measurements, only considering the polar anisotropy  $\lambda_\theta$  in one frame, as was the strategy of these Tevatron measurements, leads to major problems. Besides the ambiguity of results only stating  $\lambda_\theta$  (see Sect. 2.3.3 for more details), there are experimental pitfalls that can introduce large biases when integrating over the azimuthal component of the decay [48].

## 2.3 Quarkonium Polarization

Driven by the observed inconsistencies of the quarkonium polarization measurements at the Tevatron experiments, there has been huge progress in the understanding of quarkonium polarization and in the methodology required for the corresponding measurements. This progress was documented in a series of papers [48–53]. Some general considerations and the most important findings are discussed here. All quarkonium polarization measurements conducted at hadron colliders since the development of this new understanding follow this methodology, with the pleasant consequence that these new results show a consistent picture throughout various experiments (see Sect. 5.1.2).

### 2.3.1 General Considerations

This part is restricted to the discussion of the polarization of vector  $1^{--}$  states in the dilepton decay,  $Q^{3S_1} \rightarrow l^+ l^-$ . The polarization of the  $J^{++} \chi$  states in the radiative decays  $Q^{3P_J} \rightarrow Q^{3S_1} + \gamma$  is discussed in Sect. 2.3.4. A vector particle can be observed in three eigenstates of the angular momentum component  $J_z$ , with respect to a quantization axis  $z$ ,  $J_z = 0, \pm 1$ . If, on a statistical basis, quarkonium states are dominantly observed in either the  $J_z = 0$  or the  $J_z = \pm 1$  eigenstates, the state is called polarized, with respect to the axis  $z$ . The polarization of a quarkonium state can be interpreted as the preferred spin alignment, which can be caused by basic conservation laws and symmetries of the electroweak and strong interactions, depending on the properties of the corresponding production diagrams. A preferred spin alignment affects the decay angular distribution of the two leptons, in the quarkonium rest-frame, and can therefore be measured from this distribution. An isotropic angular decay distribution corresponds to unpolarized quarkonia, while anisotropies of the distribution reflect a polarized state. In case of preferred spin alignment corresponding to the projections  $J_z = \pm 1$ , the quarkonium is denoted as transversely polarized, in case of a preferred projection of  $J_z = 0$ , the quarkonium is denoted as longitudinally polarized. In case the quarkonium state is produced exclusively in either  $J_z = \pm 1$  or  $J_z = 0$ , the polarization is denoted as fully transverse or fully longitudinal, respectively.

The angular distribution is measured with respect to a polarization reference frame, in the quarkonium rest frame. The definitions of the polar angle  $\vartheta$  and azimuthal angle  $\varphi$  are shown in Fig. 2.9 (top). The decay angles are defined as the angles of the positive lepton with respect to the reference frame, whose  $x$ - $z$  plane is defined by the production plane (bottom left), built by joining the momentum vector of the quarkonium state with the momentum vector of the colliding beams ( $\vec{b}_1^c$  and  $\vec{b}_2^c$ ), in the laboratory frame. The  $y$  axis is defined to be perpendicular to the production plane, in the direction of  $\vec{b}_1^c \times \vec{b}_2^c$  and  $\vec{b}_2^c \times \vec{b}_1^c$ , with  $\vec{b}_1^c$  and  $\vec{b}_2^c$  defined in the quarkonium rest frame, for positive and negative rapidities, respectively.

The reference frame is then fully defined by choosing a quantization axis  $z$  within the production plane. This choice can in principle be done arbitrarily, but there are some physically motivated choices for the quantization axis with respect to which the polarization is measured, whose definitions are shown in the bottom right panel of Fig. 2.9. The HX axis is defined to be aligned with the quarkonium flight direction. The Collins-Soper axis [54] is defined as the opposite direction of the bisector of the two momentum vectors of the colliding beams, which is an approximation of the direction of the colliding partons. The third definition considered in this thesis is the Perpendicular-Helicity (PX) axis, defined to be orthogonal to the Collins-Soper axis. The definitions of the individual frames depend on the quarkonium production kinematics. In the limit of high  $p_T$  and mid-rapidity, the HX and Collins-Soper frames are orthogonal, in which case the PX and HX frames are identical. In the opposite limit of  $p_T \rightarrow 0$  and forward-rapidity, the HX and Collins-Soper frames are identical, and the HX and PX frames are orthogonal. The usage of the PX frame ensures, independently of the kinematical region of a measurement, that two orthogonal frames



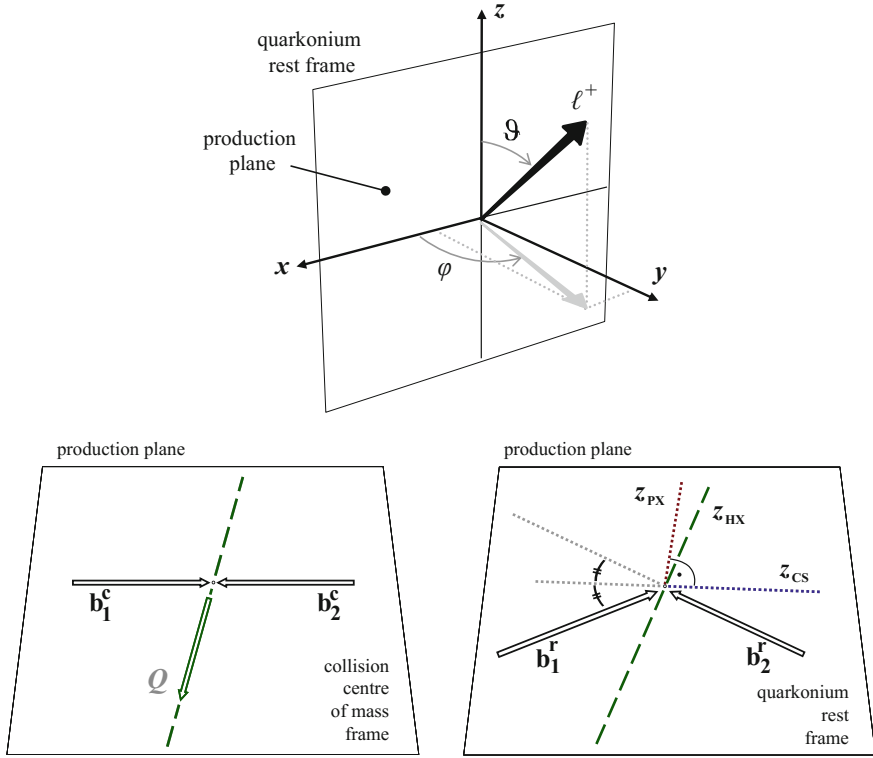


**Fig. 2.9** Definitions of the polar angle  $\vartheta$  and of the azimuthal angle  $\varphi$  of the polarization reference frame (*top*), of the production plane (*bottom left*) and of the quantization axis  $z$  (*bottom right*) [48]

can always be considered in the analysis, which is an important requirement for a reliable measurement, as argued in Ref. [49].

The angular decay distribution of a vector state can be calculated from basic quantum mechanical considerations, requiring helicity conservation at the photon-dilepton vertex of the  $Q^3S_1 \rightarrow l^+l^-$  decay. The most general angular decay distribution of a parity-conserving dilepton decay of a vector particle can be written as [48]

$$W(\cos \vartheta, \varphi | \vec{\lambda}) \propto \frac{1}{(3 + \lambda_\vartheta)} (1 + \lambda_\vartheta \cos^2 \vartheta + \lambda_\varphi \sin^2 \vartheta \cos 2\varphi + \lambda_{\vartheta\varphi} \sin 2\vartheta \cos \varphi) . \quad (2.5)$$

This distribution is parametrized by three “anisotropy parameters”  $\vec{\lambda} = (\lambda_\vartheta, \lambda_\varphi, \lambda_{\vartheta\varphi})$ , also referred to as the “polarization parameters”. The parameter  $\lambda_\vartheta$  describes the polar anisotropy of the decay,  $\lambda_\varphi$  describes the azimuthal anisotropy of the decay, and  $\lambda_{\vartheta\varphi}$  describes the change of the azimuthal anisotropy as a function of the polar angle  $\vartheta$ . The polar anisotropy parameter  $\lambda_\vartheta$  is positive (negative) in case of trans-

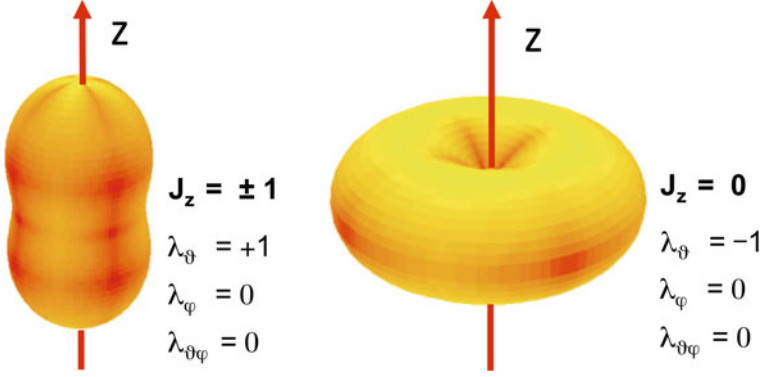


**Fig. 2.10** Fully transverse (*left*) and fully longitudinal (*right*) decay angular distributions, with respect to the quantization axis  $z$  [48]

verse (longitudinal) polarization, and  $\lambda_\vartheta = +1$  ( $\lambda_\vartheta = -1$ ) for fully transverse (fully longitudinal) vector states. Figure 2.10 shows the angular distributions for these two extreme cases, where the distance from the origin to the surface corresponds to the probability that the positive lepton is emitted in this direction.

If the angular distribution results from  $n$  samples  $i$  of vector quarkonia with different angular distributions parametrized by different anisotropy parameters,  $W(\cos \vartheta, \varphi | \vec{\lambda}^{(i)})$ , with relative weights  $f^{(i)}$ , the total angular distribution can be written as the sum  $\sum_{i=1}^n f^{(i)} W(\cos \vartheta, \varphi | \vec{\lambda}^{(i)})$ , and the effective polarization parameters, describing the inclusive angular distribution,  $\vec{\lambda}'$ , can be calculated as [48]

$$\vec{\lambda}' = \frac{\sum_{i=1}^n \frac{f^{(i)}}{3 + \lambda_\vartheta^{(i)}} \vec{\lambda}^{(i)}}{\sum_{i=1}^n \frac{f^{(i)}}{3 + \lambda_\vartheta^{(i)}}}. \quad (2.6)$$

This “polarization sum rule” is important for combining different angular distributions of feed-down decays, as well as for the addition of the polarizations of the individual color channels in NRQCD calculations. It is important to note that, in the case of several contributions characterized by different polarizations, longitudinal components carry a “heavier weight” than the transverse components. As a simple example, considering a mixture of a fully longitudinal component and a fully transverse component, with equal weights  $f^{(i)} = 0.5$ , the resulting effective polar anisotropy of the sum of the components is  $\lambda'_\vartheta = -1/3$ , very different from the unpolarized distribution that intuition might suggest.

### 2.3.2 Frame-Invariant Formalism

It is useful to introduce the concept of the “natural polarization frame”. For any decay angular distribution of a vector quarkonium state one can define a reference frame in which the polar anisotropy is maximal ( $\lambda_{\vartheta}^{nat}$ ), and in which  $\lambda_{\varphi}$  is minimal and  $\lambda_{\vartheta\varphi}$  vanishes [50]. This frame is denoted as the natural polarization frame for the given angular distribution. Each process contributing to quarkonium production, for which  $\lambda_{\vartheta}^{nat} \neq 0$ , has a natural polarization axis. With the condition that  $\lambda_{\vartheta} \in [-1, 1]$  with respect to any  $z$  axis (equivalent to the condition that the natural polar anisotropy  $\lambda_{\vartheta}^{nat} \in [-1, 1]$ ) one can derive so-called “positivity constraints” for  $\lambda_{\varphi}$  and  $\lambda_{\vartheta\varphi}$  [52], which constrain the allowed phase space of  $\vec{\lambda}$  to the regions shown as the grey areas in Fig. 2.11.

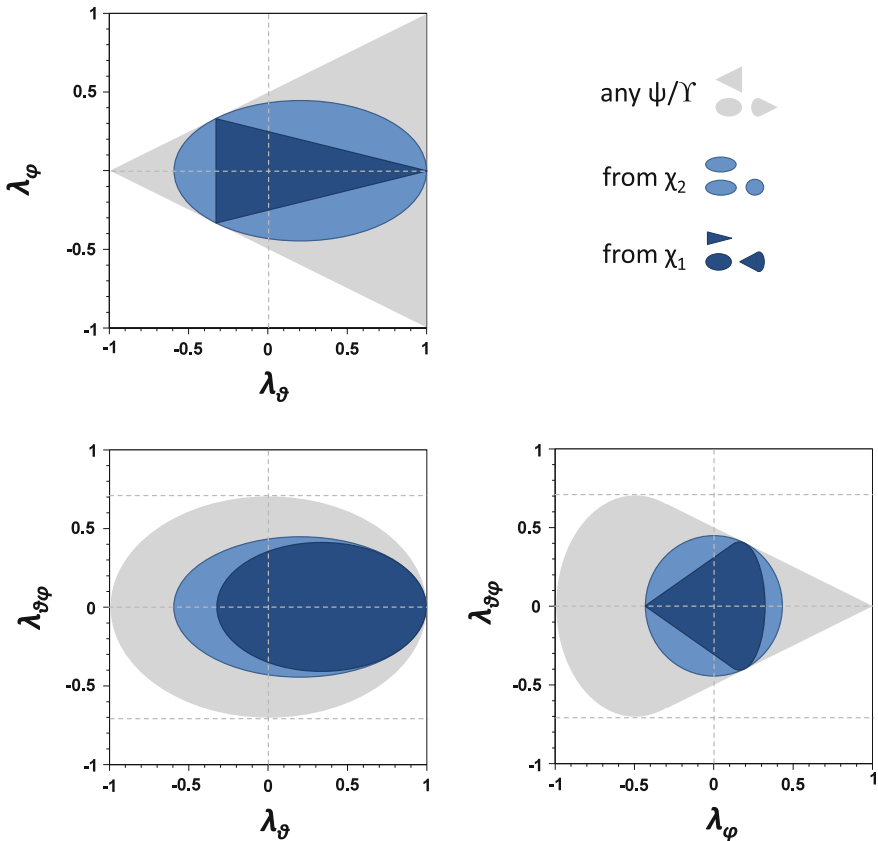


**Fig. 2.11** Allowed phase space regions of the parameters  $\vec{\lambda}$  for  $1^{--}$  (grey) and  $J^{++}$  quarkonia, with  $J = 1, 2$  (dark and light blue, respectively) [53]

The relative importance of the fundamental processes of quarkonium production can change as a function of the quarkonium kinematics, given the different  $p_T$ -slopes of the SDCs as discussed in Sect. 2.2.1, and the feed-down decays that might have varying relative importance as a function of the kinematics. Due to the different angular distributions of the individual processes, one expects a kinematic dependence of the inclusive set of parameters  $\vec{\lambda}$ , which is denoted here as “intrinsic” kinematic dependence. However, as the parameters  $\vec{\lambda}$  are frame-dependent, and as the definition of the frames depends on the kinematics, the measured polarization in a given reference frame can show a kinematic dependence simply because the measurement frame is not the natural frame, especially in cases of mixtures of processes characterized by different natural polarization axes. This dependence is denoted here as “extrinsic”, and is an artifact of the measurement, not reflecting a real physics effect, but purely kinematical effects.

Even though the parameters  $\vec{\lambda}$  are frame-dependent, the shape of the angular distribution is independent of the chosen reference frame. It is possible to define frame-invariant observables [50], as combinations of the frame-dependent parameters  $\vec{\lambda}$ . These frame-invariant quantities do not depend on the frame in which the polarization is measured, and therefore allow us to differentiate between intrinsic and extrinsic kinematic dependencies – between physics effects and purely kinematical effects. These quantities therefore carry viable physical information about the nature of the polarization of a given quarkonium state. The combination of frame-dependent and frame-invariant observables is vital, given that the frame-invariant quantities do not carry any information about the natural polarization frames.

There are an infinite number of frame-invariant observables [50] that can be defined. The most convenient parameter, widespread in the literature, is  $\tilde{\lambda}$ , defined as

$$\tilde{\lambda} = \frac{\lambda_\theta + 3\lambda_\varphi}{1 - \lambda_\varphi} . \quad (2.7)$$

This parameter is  $+1$  for any fully transverse shape and  $-1$  for any fully longitudinal shape. This means, for example, that for any mixture of processes where each component is characterized by fully transverse polarization with respect to different natural polarization axes, the resulting measurement of the inclusive sample in any frame will nevertheless result in  $\tilde{\lambda} = +1$ . Given the allowed ranges for  $\lambda_\theta$  and  $\lambda_\varphi$ ,  $\tilde{\lambda}$  is contained within the interval  $[-1, \infty]$ .

Besides its physics information, the measurement of  $\tilde{\lambda}$  provides a critical experimental cross check. The comparison of measurements of  $\tilde{\lambda}$  in several frames, including at least two orthogonal frames, can reveal systematic biases that are not accounted for in the analysis.

### 2.3.3 Ambiguity of Pre-LHC Quarkonium Polarization Measurements

The importance of following this methodology can be shown on the basis of the prompt  $J/\psi$  polarization analysis from CDF [43], which is shown in the left panel of Fig. 2.7. This measurement has been conducted before the development of the methodology as described in this section. Consequentially, the analysis was performed integrating over the azimuthal component of the decay, only providing the parameter  $\lambda_\theta$ , only in the HX frame, neither providing information about the azimuthal anisotropy, nor providing frame-invariant information through  $\tilde{\lambda}$ , which was not known at the time of the measurement.

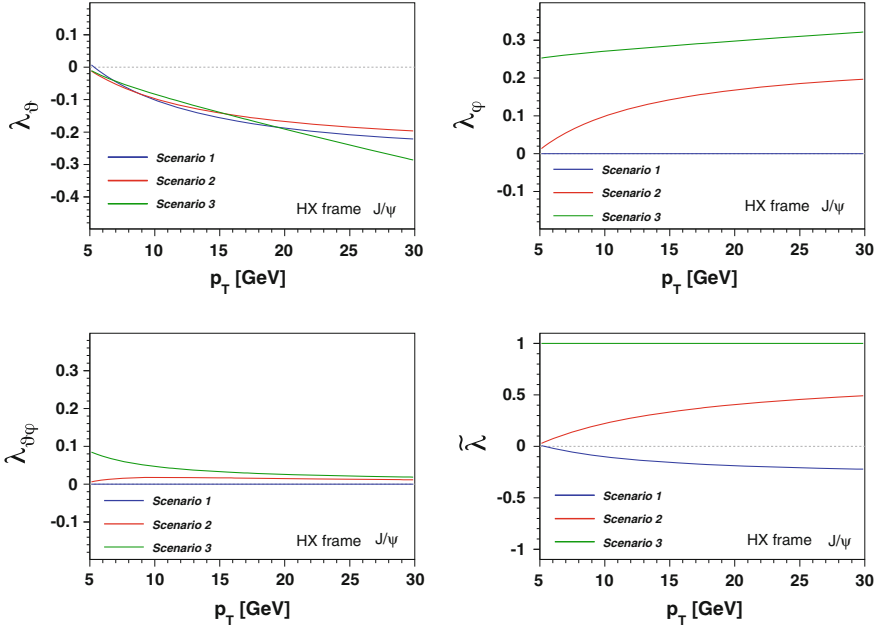
Given the unmeasured azimuthal anisotropy  $\lambda_\varphi$ , this measurement allows for several very different physical interpretations, leading to an ambiguity that can only be resolved by further measurements of the prompt  $J/\psi$  polarization, following the recipes summarized in this section. In order to visualize the ambiguity of this measurement, Ref. [55] introduces three polarization scenarios which are all compatible with the CDF measurement of  $\lambda_\theta$ , but whose 2-dimensional angular decay distributions are considerably different. The first (second) scenario assumes that the  $J/\psi$  decay angular distribution does not reveal any azimuthal anisotropy in the HX (Collins-Soper) frame,  $\lambda_\theta^{HX} = 0$  ( $\lambda_\theta^{CS} = 0$ ). The third scenario assumes a certain fraction (slightly changing as a function of  $p_T$ ) of all  $J/\psi$ 's to be produced transversely polarized with respect to the HX frame, the rest transversely polarized with respect to the Collins-Soper frame.

Figure 2.12 shows the kinematic dependence of the polarization parameters in the HX frame, for these three scenarios. This figure displays the measured parameter  $\lambda_\theta$ , showing that the individual scenarios are almost identical in  $\lambda_\theta$ , as well as the unmeasured parameters  $\lambda_\varphi$ ,  $\lambda_{\theta\varphi}$  and  $\tilde{\lambda}$ .

This pedagogical example illustrates that restricting a measurement to the polar anisotropy  $\lambda_\theta$  does not provide the necessary information to interpret the polarization of a quarkonium state, as very different physical scenarios can be compatible with such a measurement. However, if one measures also the azimuthal component and the frame-invariant parameter  $\tilde{\lambda}$ , the individual scenarios can be very easily distinguished. These calculations are further provided for the accessible rapidity ranges of the CMS detector as well as of the LHCb detector [55], allowing for an a-posteriori interpretation of the CDF results.

### 2.3.4 Polarization of the $\chi$ States

In principle, the polarizations of the P-wave quarkonia are more complicated to measure than the polarizations of S-wave quarkonia. The  $Q^{3P_J} \rightarrow Q^{3S_1} + \gamma$  decays are much more challenging to reconstruct due to the presence of a low energy photon, difficult to detect and reconstruct. The direct way to measure P-wave polarization would be to measure the angular distribution of the  $Q^{3S_1} + \gamma$  system with respect to a reference frame in the  $Q^{3P_J}$  rest frame. This is very challenging, as the photon



**Fig. 2.12** Kinematic behavior of anisotropy parameters  $\lambda_\theta$ ,  $\lambda_\varphi$ ,  $\lambda_{\theta\varphi}$  in the HX frame and  $\tilde{\lambda}$ , in the rapidity region  $|y| < 0.6$ , for the three scenarios as discussed in the text [55]

kinematics and efficiencies have to be accurately known for such studies. However, it was shown recently [53] that the  $Q^{3P_J}$  angular distribution in the  $Q^{3P_J}$  rest frame can be very well approximated by the dilepton angular distribution of the  $Q^{3S_1} \rightarrow l^+l^-$  decay in the  $Q^{3S_1}$  rest frame, for sufficiently large momenta of the original  $Q^{3P_J}$  system. For the momenta measurable by the CMS detector, the bias associated to this approximation is negligible. Therefore, the measurement of the  $J^{++}$  states can be done in the exact same way as the measurement of the  $1^{--}$  states, except for identifying those  $1^{--}$  states that are accompanied by a photon originating from the dilepton vertex, with an invariant mass close to the mass of the  $J^{++}$  state under study.

Similarly to the allowed regions for  $1^{--}$  states, one can derive the allowed regions for  $\tilde{\lambda}$  also for the  $J^{++}$  states, shown in Fig. 2.11 as the dark and light blue areas, respectively for  $J=1$  and  $J=2$ . The interpretation of the polarization of  $J^{++}$  states in terms of quantum states and preferred spin alignment is not as intuitive as the polarization of the  $1^{--}$  states. The  $1^{++}$  states have possible eigenstates corresponding to projections of the angular momentum on the  $z$ -axis of  $J_z = 0, \pm 1$ , while the  $2^{++}$  states can have the projections  $J_z = 0, \pm 1, \pm 2$ . The fully transverse polar anisotropy  $\lambda_\theta = +1$  corresponds to the  $J_z = 0$  and  $J_z = \pm 2$  eigenstates for  $J=1$  and  $J=2$  states, respectively. The partially longitudinal polar anisotropy  $\lambda_\theta = -1/3$  corresponds to the  $J_z = \pm 1$  eigenstates, for both  $J=1$  and  $J=2$  states, while the  $J_z = 0$  eigenstate of the  $J=2$  states corresponds to the minimum polar anisotropy of  $\lambda_\theta = -3/5$  [53].

## 2.4 Quarkonium Physics Summary

In this chapter the spectra of the charmonium and bottomonium meson families were introduced, followed by a discussion about the theoretical state-of-the-art framework describing quarkonium production, the NRQCD factorization approach, and a review of the situation in the field of quarkonium production physics in the pre-LHC era. The Tevatron results clarified that the color-singlet contributions cannot be solely responsible for quarkonium production in hadron collisions, and that color-octet transitions are realized in nature. However, the confusion in the quarkonium physics community was large at that time, mostly due to experimental inconsistencies in quarkonium polarization measurements. It is clear that the community eagerly awaited “better data”, and therefore an experimental clarification from the LHC experiments, especially providing quarkonium polarization data with improved and more robust analysis techniques. The LHC quarkonium physics program does not only aim at clarifying the experimental situation of quarkonium polarization, but also at extending the  $p_T$  reach of the measurements, for both production cross section measurements as well as polarization measurements, for S-wave and P-wave states, far beyond the reach of the Tevatron experiments.

The measurements at the core of this thesis have been motivated by introducing the theoretical foundation of quarkonium production physics and the existing experimental problems. The interplay of progress in theory and experiment through the LHC programs and beyond is necessary to understand the processes that lead to quarkonium production, addressing the basic and general question of how quarks bind into hadrons via the strong force.

## References

1. Olive KA et al (2014) Particle data group. Chin Phys C 38:090001
2. LHCb Collaboration (2014a) Study of  $\chi_b$  meson production in  $pp$  collisions at  $\sqrt{s} = 7$  and 8 TeV and observation of the decay  $\chi_b(3P) \rightarrow \Upsilon(3S)\gamma$ . Eur Phys J C 74:3092
3. LHCb Collaboration (2014b) Measurement of the  $\chi_b(3P)$  mass and of the relative rate of  $\chi_{b1}(1P)$  and  $\chi_{b2}(1P)$  production. J High Energy Phys 1410:88
4. ATLAS Collaboration (2012) Observation of a new  $\chi_b$  state in radiative transitions to  $\Upsilon(1S)$  and  $\Upsilon(2S)$  at ATLAS. Phys Rev Lett 108:1520012012
5. D0 Collaboration (2012) Observation of a narrow mass state decaying into  $\Upsilon(1S) + \gamma$  in  $p\bar{p}$  collisions at  $\sqrt{s} = 1.96$  TeV. Phys Rev D 86:031103
6. QWG Collaboration (2011) Heavy quarkonium: progress, puzzles, and opportunities. Eur Phys J C 71:1534
7. Belle Collaboration (2003) Observation of a narrow charmonium - like state in exclusive  $B^\pm \rightarrow K^\pm \pi^+ \pi^- J/\psi$  decays. Phys Rev Lett 91:262001
8. LHCb Collaboration (2013) Determination of the X(3872) meson quantum numbers. Phys Rev Lett 110:222001
9. Belle Collaboration (2008) Observation of a resonance-like structure in the  $\pi^\pm \psi'$  mass distribution in exclusive  $B \rightarrow K \pi^\pm \psi'$  decays. Phys Rev Lett 100:142001
10. LHCb Collaboration (2014) Observation of the resonant character of the  $Z(4430)^-$  state. Phys Rev Lett 112:222002

11. Gell-Mann M (1964) A schematic model of baryons and mesons. Phys Lett 8:214
12. Matsui T, Satz H (1986)  $J/\psi$  suppression by quark-gluon plasma formation. Phys Lett B 178:416
13. Digal S, Petreczky P, Satz H (2001) Quarkonium feed-down and sequential suppression. Phys Rev D 64:094015
14. Braun-Munzinger P, Stachel J (2000) (Non)thermal aspects of charmonium production and a new look at  $J/\psi$  suppression. Phys Lett B 490:196
15. Bodwin GT, Petriello F, Stoynev S, Velasco M (2013) Higgs boson decays to quarkonia and the  $H\bar{c}c$  coupling. Phys Rev D 88:053003
16. Bodwin GT, Braaten E, Lepage GP (1995) Rigorous QCD analysis of inclusive annihilation and production of heavy quarkonium. Phys Rev D 51:1125
17. Fritzsch H (1977) Producing heavy quark flavors in hadronic collisions – ‘A test of quantum chromodynamics’. Phys Lett B 67:217
18. Private communication from P. Faccioli
19. Butenschön M, Kniehl B (2012)  $J/\psi$  polarization at Tevatron and LHC: Nonrelativistic-QCD factorization at the crossroads. Phys Rev Lett 108:172002
20. Schuler GA (1997) Quarkonium production: Velocity scaling rules and long distance matrix elements. Int J Mod Phys A 12:3951
21. Price DD (2008) Studies of quarkonium production and polarisation with early data at ATLAS. Ph.D. thesis, Lancaster University
22. Artoisenet P, Lansberg JP, Maltoni F (2007) Hadroproduction of  $J/\psi$  and  $\Upsilon$  in association with a heavy-quark pair. Phys Lett B 653:60
23. Campbell JM, Maltoni F, Tramontano F (2007) QCD corrections to  $J/\psi$  and Upsilon production at hadron colliders. Phys Rev Lett 98:252002
24. Gong B, Wang JX (2008) Next-to-leading-order QCD corrections to  $J/\psi$  polarization at Tevatron and Large-Hadron-Collider energies. Phys Rev Lett 100:232001
25. Gong B, Wang JX (2008) QCD corrections to polarization of  $J/\psi$  and  $\Upsilon$  at Tevatron and LHC. Phys Rev D 78:074011
26. Gong B, Li XQ, Wang JX (2009) QCD corrections to  $J/\psi$  production via color octet states at Tevatron and LHC. Phys Lett B 673:197
27. Ma YQ, Wang K, Chao KT (2011) QCD radiative corrections to  $\chi_{cJ}$  production at hadron colliders. Phys Rev D 83:111503
28. Artoisenet P, Campbell JM, Lansberg JP et al (2008)  $\Upsilon$  production at Fermilab Tevatron and LHC energies. Phys Rev Lett 101:152001
29. Lansberg JP (2009) Real next-to-next-to-leading-order QCD corrections to  $J/\psi$  and Upsilon hadroproduction in association with a photon. Phys Lett B 679:340
30. Aubert JJ et al (1974) Experimental observation of a heavy particle  $J$ . Phys Rev Lett 33:1404
31. Augustin JE et al (1974) Discovery of a narrow resonance in  $e^+e^-$  annihilation. Phys Rev Lett 33:1406
32. Kartvelishvili VG, Likhoded AK, Slabospitsky SR (1978)  $D$  meson and  $\psi$  meson production in hadronic interactions. Sov J Nucl Phys 28:678
33. Baier R, Ruckl R (1983) Hadronic collisions: a quarkonium factory. Z Phys C 19:251
34. Glover EW, Martin AD, Stirling WJ (1988)  $J/\psi$  production at large transverse momentum at hadron colliders. Z Phys C 38:473
35. E789 Collaboration (1995) Measurement of  $J/\psi$  and  $\psi'$  production in 800-GeV/c proton-gold collisions. Phys Rev D 52:1307
36. McGaughey PL (1996) Recent measurements of quarkonia and Drell-Yan production in proton nucleus collisions. Nucl Phys A 610:394C
37. CDF Collaboration (1997)  $J/\psi$  and  $\psi(2S)$  production in  $p\bar{p}$  collisions at  $\sqrt{s} = 1.8$  TeV. Phys Rev Lett 79:572
38. Krämer M (2001) Quarkonium production at high-energy colliders. Progr Part Nucl Phys 47:141
39. CDF Collaboration (1996) Quarkonia production at CDF. Nucl Phys A 610:373C



40. CDF Collaboration (1997) Production of  $J/\psi$  mesons from  $\chi_c$  meson decays in  $p\bar{p}$  collisions at  $\sqrt{s} = 1.8$  TeV. *Phys Rev Lett* 79:578
41. Braaten E, Kniehl B, Lee J (2000) Polarization of prompt  $J/\psi$  at the Tevatron. *Phys Rev D* 62:094005
42. CDF Collaboration (2000) Measurement of  $J/\psi$  and  $\psi(2S)$  polarization in  $p\bar{p}$  collisions at  $\sqrt{s} = 1.8$  TeV. *Phys Rev Lett* 85:2886
43. CDF Collaboration (2007) Polarization of  $J/\psi$  and  $\psi(2S)$  mesons produced in  $p\bar{p}$  collisions at  $\sqrt{s} = 1.96$  TeV. *Phys Rev Lett* 99:132001
44. Butenschön M, Kniehl B (2012)  $J/\psi$  production in NRQCD: a global analysis of yield and polarization. *Nucl Phys B Proc Suppl* 151:222–224
45. Lansberg JP (2011)  $J/\psi$  production at  $\sqrt{s} = 1.96$  and 7 TeV: color-singlet model, NNLO\* and polarisation. [arXiv:1107.0292](https://arxiv.org/abs/1107.0292)
46. CDF Collaboration. CDF public note 9966
47. D0 Collaboration (2008) Measurement of the polarization of the  $\Upsilon(1S)$  and  $\Upsilon(2S)$  states in  $p\bar{p}$  collisions at  $\sqrt{s} = 1.96$  TeV. *Phys Rev Lett* 101:182004
48. Faccioli P, Lourenço C, Seixas J, Wöhri H (2010) Towards the experimental clarification of quarkonium polarization. *Eur Phys J C* 69:657
49. Faccioli P, Lourenço C, Seixas J, Wöhri H (2009)  $J/\psi$  polarization from fixed-target to collider energies. *Phys Rev Lett* 102:151802
50. Faccioli P, Lourenço C, Seixas J (2010a) Rotation-invariant relations in vector meson decays into fermion pairs. *Phys Rev Lett* 105:061601
51. Faccioli P, Lourenço C, Seixas J (2010b) A new approach to quarkonium polarization studies. *Phys Rev D* 81:111502
52. Faccioli P, Lourenço C, Seixas J, Wöhri H (2011a) Model-independent constraints on the shape parameters of dilepton angular distributions. *Phys Rev D* 83:056008
53. Faccioli P, Lourenço C, Seixas J, Wöhri H (2011b) Determination of  $\chi_c$  and  $\chi_b$  polarizations from dilepton angular distributions in radiative decays. *Phys Rev D* 83:096001
54. Collins JC, Soper DE (1977) Angular distribution of dileptons in high-energy hadron collisions. *Phys Rev D* 16:2219
55. Knünz V (2011) Measurement of  $J/\psi$  polarization with the CMS experiment in proton-proton collisions at  $\sqrt{s} = 7$  TeV. Diploma Thesis, Institute of High Energy Physics, Vienna University of Technology

Measurement of Quarkonium Polarization to Probe QCD  
at the LHC

Knuenz, V.

2017, XVII, 166 p. 74 illus., 37 illus. in color., Hardcover

ISBN: 978-3-319-49934-5